Coacervation Induced Remodeling of Nanovesicles

Sayantan Mondal[†] and Qiang Cui*,†,‡,¶

†Department of Chemistry, Boston University, 590 Commonwealth Avenue, Boston, MA 02215, United States

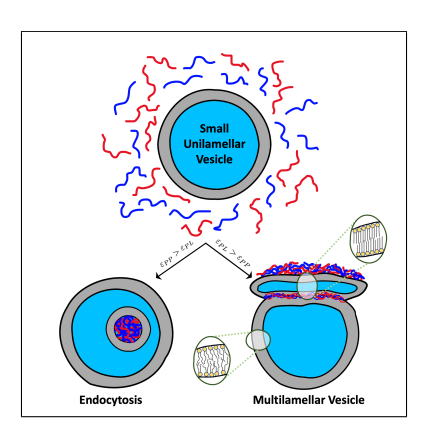
‡Department of Physics, Boston University, 590 Commonwealth Avenue, Boston, MA
02215, United States

 \P Department of Biomedical Engineering, Boston University, 44 Cummington Mall, Boston, MA 02215, United States

E-mail: qiangcui@bu.edu,Tel:(+1)-617-353-6189

Abstract

Intrinsically disordered peptides can form biomolecular condensates through liquid-liquid phase separation. These condensates play diverse roles in cells, including inducing large-scale changes in membrane morphology. Here we employ coarse-grained molecular dynamics simulations to identify the most salient physical principles that govern membrane remodeling by condensates. By systematically varying the interaction strengths among the polymers and lipids in our coarse-grained model, we are able to recapitulate various membrane transformations observed in different experiments. Endocytosis and exocytosis of the condensate are observed when the inter-polymeric attraction strength is higher than polymer-lipid interaction. We find a critical size of the condensate required to exhibit successful endocytosis. Multilamellarity and local gelation are observed when the polymer-lipid attraction is significantly higher than the inter-polymeric attraction. The insights provide essential guidance to the design of (bio)polymers for the manipulation of membrane morphology in various applications such as drug delivery and synthetic biology.



TOC graphic

Liquid-liquid phase separation (LLPS) of intrinsically disordered peptides (IDPs) and nucleic acids is an important biological process that is connected to intracellular compartmentalization through the formation of membraneless organelles (such as nucleoli, stress granules, cajal bodies etc.), cellular signaling, and several diseases.^{1–7} In the last decade, there has been a tremendous advancement in understanding the formation, structure and dynamics of such macromolecular condensates in the bulk phase, both theoretically and experimentally. Recent studies have suggested that LLPS at the lipid membrane is biologically important.^{8–12} It was also observed that phase separation of proteins at the membrane surface can induce significant curvatures, vesicle biogenesis, multilamellar structure formation, tubulation, and pore formation.^{13–19} Therefore, LLPS near the membrane surface can serve as a novel mechanism for membrane remodeling in cells, in addition to the much discussed mechanisms such as hydrophobic insertion, scaffolding, protein crowding, and coating.^{20–22} Despite the importance and interest in general, only a few theoretical investigations have been directed toward understanding the mechanism of LLPS-induced large-scale structural transformations of a lipid bilayer or vesicle, from a molecular perspective.

Membranes can modulate the structure and, in turn, the phase boundaries of the condensate. For example, the conformational ensemble of a single IDP chain close to a membrane can differ largely from that in the bulk.^{23,24} As the single chain properties are known to be well correlated with the phase behavior of the condensate, ^{25–28} in such cases, the membrane can introduce changes in the protein phase behavior that is non-trivial to predict by only considering the enhanced local protein concentration due to membrane adsorption.⁸ In addition, there can be coupling between phase behaviors of the peripheral proteins and the lipid membrane.^{29,30} In a lattice model-based study, Machta *et al.* showed that membranes close to the critical point can promote protein phase separation on its surface, even if LLPS is unfavorable in the bulk;³¹ we recently further showed using similar approaches that the critical behavior of the membrane is not required to promote the pre-wetting transition of biopolymers at the membrane surface.³² Continuum mechanics models have been used to

rationalize membrane bending and tubulation upon adsorption of a dense protein layer, ^{14,19} although molecular details for the underlying driving force were difficult to establish using such models alone.

Mixtures of oppositely charged polyelectrolytes readily undergo LLPS and are often termed as coacervation. 33-35 These coacervates have a wide range of applications from coatings and adhesives to pharmaceutical technologies and foster multiple biological processes. 36-40 Polyelectrolyte coacervates are used to build synthetic analogs of living cells (protocells) owing to their crowded interior, unique core-shell property, and molecular sequestration capability. 41,42 Recent experimental studies have observed several biologically important phenomena caused by the adsorption of coacervates onto a lipid vesicle/membrane. For example, Spruijt and co-workers have used timelapse fluorescent microscopy to observe endocytosis and exocytosis of spermine/poly-Uracil coacervate droplets. 17 The lipid coating followed by the engulfment of the coacervate into the liposome has been first observed within 15s. Throughout the length of their experiment (20 min) they observed the engulfment of several droplets. By varying the concentration of positively (DOTAP) and negatively (POPG) charged lipids, that is, tuning the strength of interaction between the droplet and liposome, they presented a qualitative phase diagram based on contact angles. Another interesting earlier study by Allolio et al. showed that poly-Arginine can induce the formation of fused multilamellar bilayer structure followed by membrane pore formation. 18 Inspired by these and other 14,43-45 experimental observations, we aim to unravel which intra/inter-molecular interactions are the key to the experimental observations of large-scale membrane remodeling processes such as endocytosis, exocytosis, and multilamellar bilayer formation. In other words, we aim to provide a molecular level explanation of the schematic phase diagram of a coacervate-liposome system presented by Spruijt and co-workers. 17 We believe such understanding based on molecular interactions is required to help design novel synthetic polymers to achieve the desired outcome of vesicle remodeling. The use of model systems by a systematic tuning of self- and cross-interaction strengths has been used to understand the nature of LLPS in the bulk, 46,47

but not in the presence of a liposome.

Given the timescale of these processes, one often resorts to coarse-graining approaches ^{26,48–51} or numerical solutions of field theory-based equations. ^{3,52} Here we use the generic three-bead representation for lipid molecules proposed by Cooke et al. ⁴⁹ and model polymers made of self-repulsive beads to identify the most salient features in intermolecular interactions that drive the experimentally observed diverse phenomena. We note that the Cooke model for lipids was used earlier in several studies to understand the passive uptake of nanoparticles through a flat bilayer and its dependence on the shape and size of the nanoparticle. ^{53,54} However, the effect of LLPS on a vesicle made of Cooke lipids has not been investigated. The primary difference between nanoparticle uptake and the endocytosis of coacervates is the entropic factor, as the individual chains can exhibit substantial conformational fluctuations and intermolecular rearrangements within the coacervate, making it spatially inhomogeneous in terms of both structure and dynamics. ⁵⁵ In addition, unlike the nanoparticles, the coacervates exhibit shape and volume fluctuations that can be manifested into interesting structural features that are often unanticipated.

We have three components in the system, namely, the lipid vesicle made out of a single component and two polymers A_{30} and B_{30} . The following parameterization and details are in the reduced unit. The lipids have one head bead (H) and two tail beads (T) with diameters $\sigma_{HH} = 0.95 = \sigma_{HT}$ and $\sigma_{TT} = 1.00$. The pair interaction between H-H and also between H-T are repulsive Weeks-Chandler-Andersen (WCA) type with $\varepsilon = 1$ and $r_c = 2^{1/6}\sigma$ [Eq. (1)].

$$U_{WCA}(r) = 4\varepsilon \left[(\sigma/r)^{12} - (\sigma/r)^6 + (1/4) \right] \quad , r \le r_c$$

$$= 0 \qquad \qquad , r > r_c$$

$$(1)$$

However the interaction between the 'T' beads are a combination of a truncated Lennad-Jones and cosine potential as given in Eq. (2) where $\varepsilon = 1$, $r_c = 2^{1/6}\sigma_{TT}$, and $w_c = 1.6\sigma_{TT}$.

$$U_{TT}(r) = -\varepsilon \qquad , r < r_c$$

$$= -\varepsilon \cos^2 \frac{\pi (r - r_c)}{2w_c} \quad , r_c \le r \le (r_c + w_c)$$

$$= 0 \qquad , r > (r_c + w_c)$$

$$(2)$$

We keep the intermolecular interaction of the lipids intact as suggested in the original study by Cooke et al.⁴⁹ The beads are linked by two FENE bonds [Eq. 3] with k=30 and $r_{\infty}=1.5$

$$V_{FENE}(r) = -\frac{1}{2}kr_{\infty}^{2}log[1 - (r/r_{\infty})^{2}].$$
 (3)

In addition, between the head and the second tail bead there is a harmonic potential with k=10 and $r_0=4\sigma$. The vesicle is constructed with a total of 20,090 CG lipids with a diameter of 70 reduced units (8,125 in the inner leaflet and 11,965 in the outer leaflet). The polymer beads are self-repulsive, that is, the interaction between A-A and B-B are of the WCA type [Eq. (1)] with $\varepsilon=1$ and $\sigma_{AA}=0.50=\sigma_{BB}$. The consecutive beads in a single polymer chain are connected by harmonic bonds with a force constant of k=50.0 and an equilibrium bond distance of $r_0=0.548$. The interaction between A-T and B-T are also of the WCA type. However, the inter-polymeric interaction between A and B are Lennard-Jones (LJ) type attractive interaction as given by [Eq. (4)] with $r_c^{LJ}=2.5\sigma$. The interaction between the polymer bead and the lipid 'H' beads are also attractive LJ type and described by [Eq. (4)].

$$U_{LJ}(r) = 4\varepsilon \left[(\sigma/r)^{12} - (\sigma/r)^{6} \right] \quad , r \le r_c^{LJ}$$

$$= 0 \qquad \qquad , r > r_c^{LJ}$$

$$(4)$$

The strength of the LJ interactions are tuned and several combinations of ε_{AB} , ε_{AH} , and ε_{BH} are simulated out of which we report five systems as detailed in Table 1. A description of the individual components of the systems and the corresponding interactions are given in

Figure 1(a).

Table 1: Lennard-Jones interaction strengths across different systems; between A-B, A-H, and B-H.

ε_{AB}	ε_{AH}	ε_{BH}
1.0	1.0	1.0
1.0	1.0	2.0
2.0	1.0	1.0
1.0	2.0	2.0
2.0	2.0	2.0
	1.0 1.0 2.0 1.0	1.0 1.0 1.0 1.0 2.0 1.0 1.0 2.0

We have prepared the vesicle with packmol. 56 The vesicle was then placed at the center of a $(100 \ unit)^3$ cubic box. The polymer chains A_{30} and B_{30} , 100 of each, were placed randomly inside the box [Figure 1(b)]. We have simulated the systems using the LAMMPS simulation package by utilizing the customized tabulated potential. 57,58 The simulations are performed with no additional solvent or ion beads. The systems were first energy minimized with the fire algorithm followed by equilibration for 10^5 steps with dt*=0.002. During the equilibration, the temperature(T*) was slowly taken to 1.1 starting from a Maxwell distribution at T*=0.8. We then perform Langevin dynamics with T*=1.1, dt*=0.005, and a damping timescale of 50 for 5×10^7 steps. The coordinates and energies are written every 5000 steps. We use Visual Molecular Dynamics (VMD 1.9.3) for visualization purposes. 59

Here, the coarse-graining length-scale typically corresponds to $\sigma = 0.693 \ nm$. Hence, the simulated vesicle corresponds to a vesicle of diameter 50 nm in reality. The polymers, on the other hand, are modeled with oppositely charged polyelectropytes (such as, Glu_{30} and Lys_{30} ; or many other pairs) in mind. Therefore, the bead to bead distance corresponds to 0.38 nm which is the typical $C_{\alpha} - C_{\alpha}$ distance in the CHARMM36m force-field description. ⁶⁰

In system-1, the interaction parameters are such that the polymers cannot distinguish between its conjugate polymer chain and a lipid head group. Hence, we observe adsorption of both of the polymers on the vesicle uniformly. The polymers do not tend to form a coacervate or remodel the shape of the vesicle [Figure 1(c)]. In system 2, one of the polymers

 (B_{30}) is more attractive towards the head groups ($\varepsilon_{BH} = 2.0$), whereas the interpolymeric interactions and the interaction between A_{30} and lipid heads are weaker ($\varepsilon_{AB} = 1.0 = \varepsilon_{AH}$). In this case, the polymer chains containing B-type beads (colored in Orange in Figure 1) preferentially adsorb on the vesicle. The other set of polymers containing A-type beads (colored in Green in Figure 1) mostly adsorb on top of the already adsorbed layer of B_{30} . Again, we do not observe any sign of vesicle remodeling [Figure 1(d)]. Thus the polymers are capable of forming a 'coat' around cell membranes without affecting the cell morphology, which protects them from harsh environmental conditions. ^{61,62} This is used in the preservation of delicate food items that increase their shelf-life.

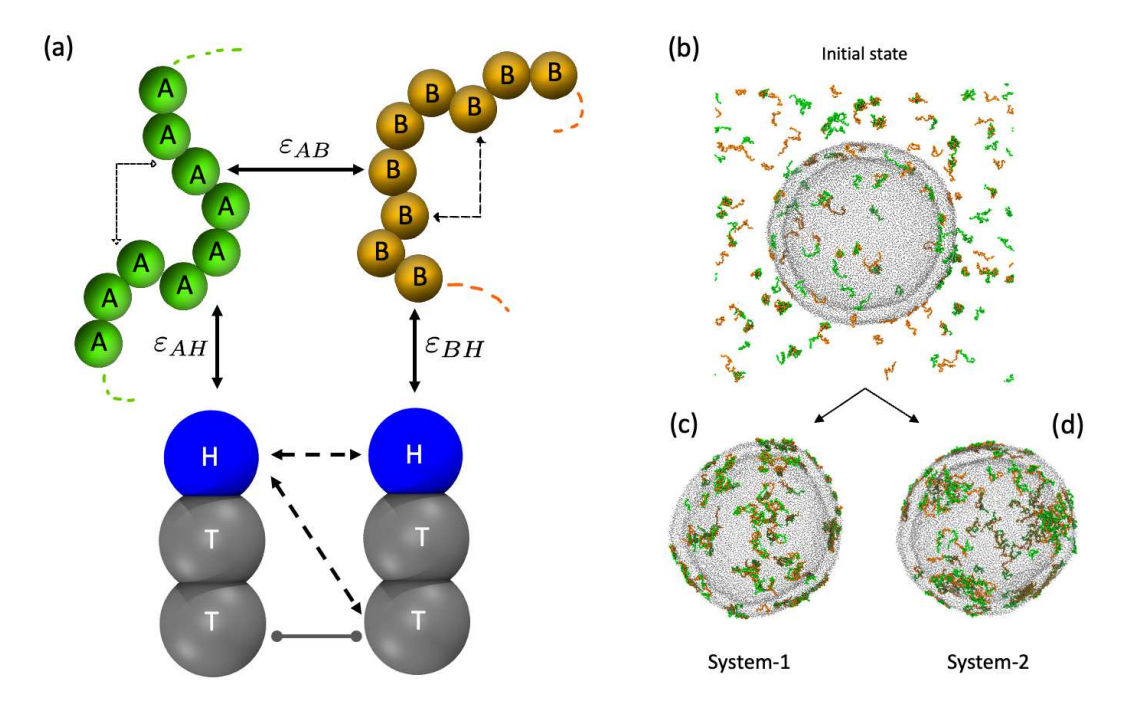


Figure 1: (a) Different components of the model system and the corresponding interactions. A and B are two kinds of polymer beads. H and T are, respectively, the head and tail beads in the Cooke lipid model. The attractive interactions are shown by solid lines and repulsive interactions are shown by broken lines. (b) Initial condition of the system where the polymers are distributed randomly around the vesicle. Adsorption of the polymers on the bilayer vesicle for (c) system 1 and (d) system 2, starting from the initial random configuration. After adsorption, in both systems, the polymers cannot visibly remodel the shape of the vesicle.

System-3, where the interpolymeric attractive interaction is twice that of polymer-lipid

interactions, leads to several interesting observations. As shown in Figure 2(a), starting from a randomly distributed polymer configuration outside the vesicle, we observe several events of endocytosis. The sequence of the observed dynamical events are as follows. First the polymer pairs undergo scattered adsorption on the outer layer of the vesicle, followed by partial association through surface mediated diffusion to form larger coacervate droplets. Once a critical size of the droplet (R_c) is surpassed, the droplets start to generate negative curvature and eventually get engulfed by the bilayer that leads to endocytosis, similar to the experimental observations of Spruijt and co-workers.¹⁷

During our simulation, we observe the endocytosis of three such coacervate droplets and the fourth one stays outside after creating a prominent negative curvature, as seen in Figure 2(a). To determine R_c , we have performed several simulations by systematically changing the number of polymers (denoted by 'N' in Figure 3(a)) in the coacervate, for system-3. We observe that coacervates with any number of polymers can partially wet the membrane and create a negative curvature. However, only coacervates with $N \geq 46$ ($R_c = 3.5 \ units$) can exhibit successful events of endocytosis. Interestingly, for N = 44 we observe an intermediate where the coacervate is fully coated with lipids, but did not exhibit endocytosis [Figure 3(a)].

We also perform a simulation with the same system but with the polymers randomly distributed *inside* the vesicle [Figure 2(b)]. The polymers form small clusters that emerge into larger coacervates. The coacervates then induce a negative curvature (from the lumen's perspective) and form buds. We, however, find that the buds (or the wrapped configuration) are stable and do not exhibit spontaneous exocytosis within the timescale explored in our simulations.

To gain more microscopic insight to the process, and partly to bypass the scattered adsorption process, we perform simulations with preformed coacervate as shown in Figure 2(c) and 2(d). The coacervate is generated from a separate polymer-only simulation with the same parameters and settings. In one system, we put the coacervate outside the vesicle

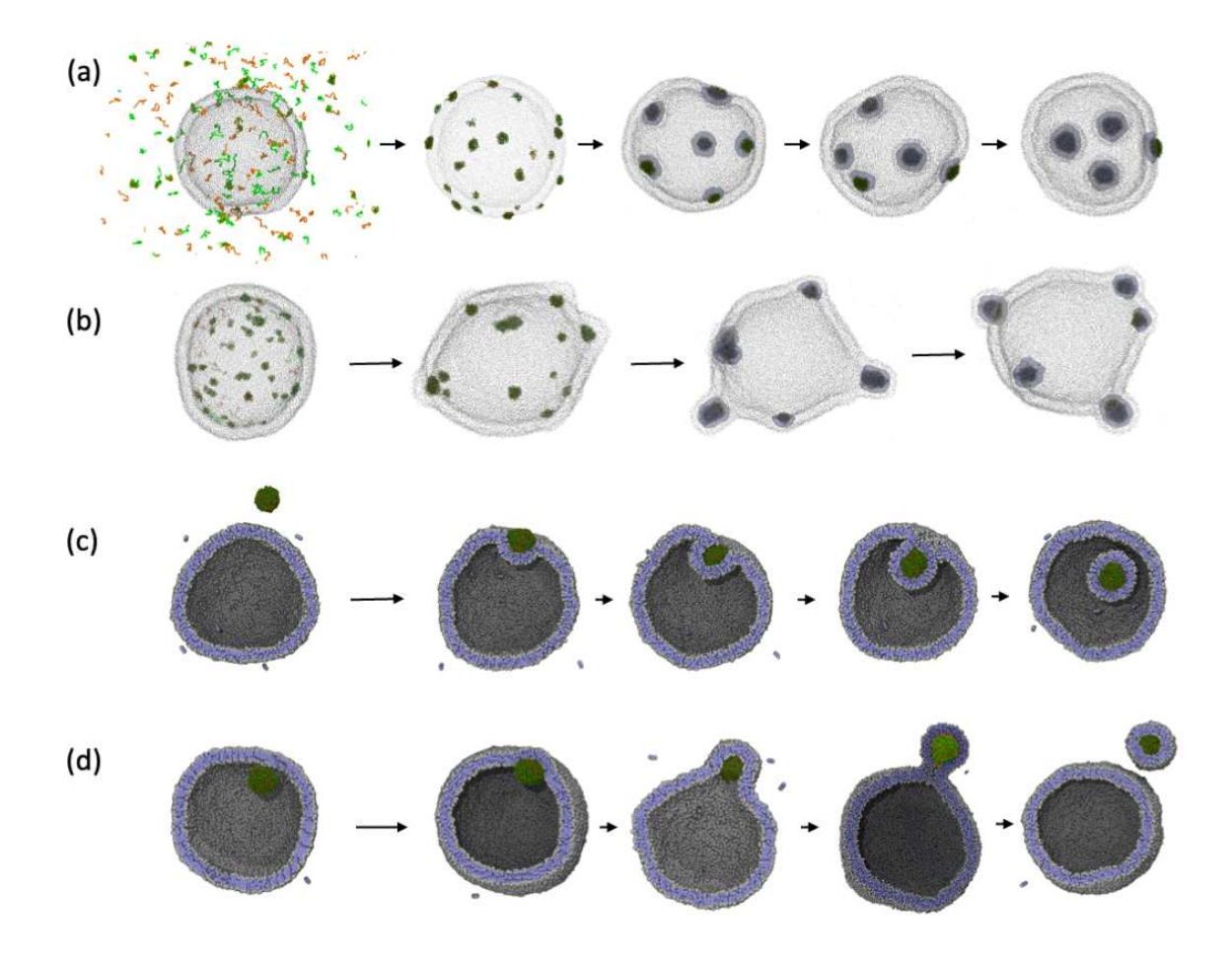


Figure 2: Snapshots of system-3 where endocytosis and exocytosis are observed. Multiple events of (a) endocytosis of coacervate droplets starting from the initial random configuration. The polymers show scattered adsorption on the outer vesicle surface, followed by partial association to increase their size, and finally endocytosis after creating a negative curvature. (b) Bud and neck formation of the vesicle by coacervate droplets when the polymers are randomly placed in the interior part of the vesicle. (c) Endocytosis and (d) Exocytosis of a preformed coacervate. The two types of polymer beads are shown in green and red, the lipid heads are shown in grey, and the tails are shown in mauve. The observed stages of endocytosis are adsorption, negative curvature generation, engulfment, and finally insertion of the coacervate coated with lipid bilayer. For exocytosis, the observed stages are adsorption, negative curvature generation, bud formation, and finally detachment of the coacervate spherically coated with the lipid bilayer. The respective movies are provided in **Supporting Information** [Video S1, S2, S3 and S4 for Figures 2(a), 2(b), 2(c), and 2(d), respectively.]

and in the other, inside the vesicle. In the former, we observe the following sequence of events: (i) adsorption of the droplet on the vesicle, (ii) negative curvature generation, (iii) engulfment of the coacervate by the vesicle, and finally (iv) endocytosis [Figure 2(c)]. After

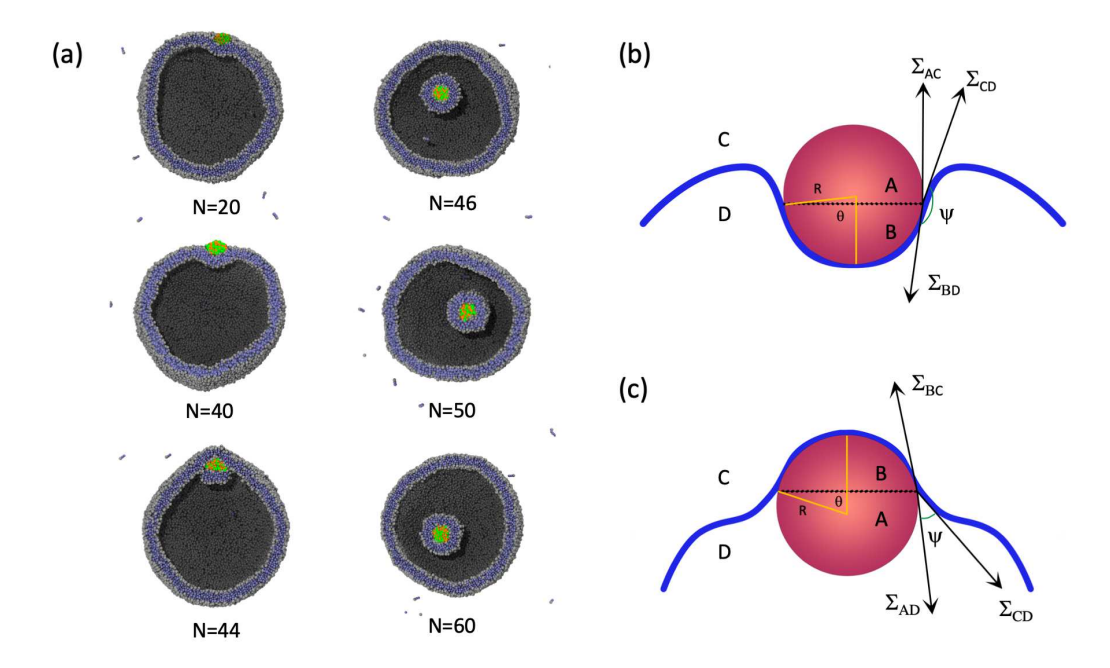


Figure 3: (a) Dependence of endocytosis on the size or concentration of the coacervate for system 3. Here N is the total number of polymer chains which means N/2 A_{30} and N/2 B_{30} . Up to N=40 the coacervate induces negative curvature at the outer surface of the vesicle without exhibiting endocytosis. For N=44 the coacervate coats itself with lipids but does not exhibit endocytosis. However, for $N \geq 46$ the event of endocytosis is observed within 10^7 simulation steps. Schematic surface tension balance diagrams for (b) endocytosis and (c) exocytosis.

the completion of the process, the diameter of the smaller vesicle containing the coacervate becomes \sim 20 reduced units (\sim 14 nm) whereas, the diameter of the original vesicle becomes \sim 60 reduced unit (\sim 41 nm).

In the simulation where the coacervate is placed inside the vesicle, the sequence of events is as follows: (i) Adsorption of the coacervate in the inner layer of the vesicle, (ii) negative curvature generation, (iii) bud formation, (iv) necking of the bud, and (v) detachment of the coacervate wrapped in bilayer through exocytosis [Figure 2(d)]. The sizes of the smaller and larger vesicles are comparable to those of endocytosis [Figure 2(c)]. However, we find that the neck in this case is more stable and the shape of the coacervate becomes teardrop-like, rather than spherical as observed for the endocytosis process. The teardrop shape allows more contact area between the polymers and the vesicle, leading to enthalpic stabilization.

The final detachment takes a sufficiently longer time in exocytosis ($\sim 6.8 \times 10^6$ steps) than endocytosis ($\sim 3.5 \times 10^5$ steps).

We aim to explain the size dependence and also the difference in the stability of the intermediate during endocytosis and exocytosis by employing existing theoretical frameworks. For these processes to be successful, a competition predominantly involves the bending energy of the membrane (κ) , the adhesion strength of the polymeric condensate per unit area (α) , and the lateral tension of the membrane (σ) . In the context of nanoparticle engulfment, a relation between the critical size (R_c) , κ , α , and σ exists in the literature. ⁶³ If we consider the schematics shown in Figure 3(b) and 3(c), one can define an order parameter: $z = 1 - \cos\theta$. Therefore, when $\theta \to \pi$ $(or, z \to 2)$ the condensate is totally engulfed. For such a system, the energy balance equation is given by Eq.(5).

$$E_{adhesion} = E_{bending} + E_{stretch}$$

$$or, 2z\pi R^2 \alpha = 4z\pi \kappa + z^2 \pi R^2 \sigma$$
(5)

From Eq.(5), by substituting z = 2 for complete engulfment $(R = R_c)$, Eq.(6) can be obtained

$$R_c = \sqrt{\frac{2\kappa}{\alpha - \sigma}} \approx \sqrt{\frac{2\kappa}{\alpha}} \ (for \ negligible \ E_{stretch})$$
 (6)

From our simulation results shown in Figure 3(a), by taking $\kappa = 20~k_BT$ and $R_c = 3.5~units$, α turns out to be 3.26, which is a reasonable estimate.⁶⁴

Next we establish the condition for endocytosis and exocytosis with respect to different interfacial tensions. Let us consider an intermediate during endocytosis [Figure 3(b)] where we identify four different phases: (i) A, the portion of the unwrapped condensate, (ii) B, the portion of the wrapped condensate, (iii) C, exterior of vesicle, and (iv) D, interior of vesicle. The rationale behind considering two regions within the condensate is as follows. Due to the inherent heterogeneity of the condensate⁵⁵ and partial interaction with the lipids, the wrapped and unwrapped portions can have different densities and fluctuation properties. In

such a scenario, the angle ψ can be expressed by Neuman's equation [Eq.(7)].

$$cos\psi = \frac{\Sigma_{AC}^2 - (\Sigma_{CD}^2 + \Sigma_{BD}^2)}{2\Sigma_{CD}\Sigma_{BD}}$$
 (7)

Starting from an unwrapped state, for a full engulfment and endocytosis, the angle ψ gradually varies from π to 0; that is, the surface tension of coacervate-exterior interface has to be greater than the sum of the surface tensions of bilayer-interior and coacervate-bilayer tensions. When $\psi = 0$, Eq.(7) yields

$$\Sigma_{AC} = \Sigma_{CD} + \Sigma_{BD} \tag{8}$$

Similarly, for exocytosis [Figure 3(c)] one can write down the appropriate Neuman's equation and show that the full engulfment ($\psi = \pi$) is achieved when

$$\Sigma_{BC} = \pm (\Sigma_{CD} - \Sigma_{AD}) \tag{9}$$

The estimates of surface tension can vary over several orders of magnitudes. The surface tension of complex coacervates can be $\sim 10\text{-}1000~\mu\text{N/m}^{65,66}$ whereas, that of a lipid bilayer is $\sim 0.1\text{-}10~\mu\text{N/m}.^{17,67}$ Therefore, Σ_{AC} and Σ_{AD} in Eq.(8) and Eq.(9) respectively, could surpass the rest. Hence, in Eq.(9) only one solution is valid, that is, $\Sigma_{BC} = (\Sigma_{AD} - \Sigma_{CD})$.

Earlier studies by Weikl and co-workers on the role of membrane curvature in the engulfment of nanoparticles revealed that endocytosis passes through an unstable intermediate whereas exocytosis passes through a neck forming stable intermediate. ⁶⁴ We observe the same in our simulations [Figure 2(d)] where the detachment of the bud is slow and driven by thermal fluctuations as the process is not energetically downhill. According to their phase diagram, for a spherical particle initially inside the vesicle, the partially wrapped and fully wrapped states are stable for higher values of the adhesion energy α . As most of the naturally occurring IDPs contain a substantial fraction of charged residues, the high value

of α is possible. Therefore, in reality, vesicle necks and buds can be sustained which is needed for intracellular protein sorting, storage vacuoles, and also in the generation of stable multi-spherical shapes that can form membrane tubules.⁶⁸

The remaining two systems (systems 4 and 5) exhibit the formation of multilamellar bilayer structures out of a spherical vesicle, as shown in Figures 4(a) and 4(c). In Figures 4(b) and 4(d) we show the cross-sectional and magnified views of the multilamellar structure. We find that in these systems, the spherical shape of the coacervate is not retained. The polymers spread out and fold the bilayer around them to maximize the polymer-lipid contact. Such folding of the bilayer and emergence of the multilamellar structure was also reported by Allolio et al. by poly-arginine rich peptides prior to pore formation. Although pore formation is not observed from our models, the predominant molecular interactions necessary to form multilamellar vesicular structure are underscored.

Interestingly, here we also discover an enhanced local gel-like ordering of the lipid tails in the vicinity of the polymer coatings where the other parts show liquid-like disordered tails [Figure 4(b) and 4(d)]. This happens to increase the polymer-lipid contact as gelation reduces the area per lipid.⁶⁹ Therefore, a larger number of lipids can be packed in the vicinity of the polymers which provides enthalpic stabilization at the cost of entropy loss. In an earlier experimental study, Wang et al. hypothesized similar gel-like patch formations in zwitterionic lipid vesicles by the adsorption of negatively charged polystyrene nanoparticles.⁴³ Recently, Stachowiak and co-workers have shown that LLPS of the RGG domain of LAF-1 can produce ordered lipid regions.⁴⁴ In system-4, the gel-like ordering is observed for bilayers surrounded by polymers from both leaflets whereas, in system-5 the gel-like ordering happens with only one leaflet coated with the polymers. The only difference between these two systems is the inter-polymeric interaction strength which is manifested in the induced gelation of the lipids.

Endocytosis and exocytosis are important processes of membrane trafficking that are required for bulk transport. The former helps the cell to take nutrients for cellular growth, function, and repair; whereas the latter helps the cell to excrete, migrate, communicate,

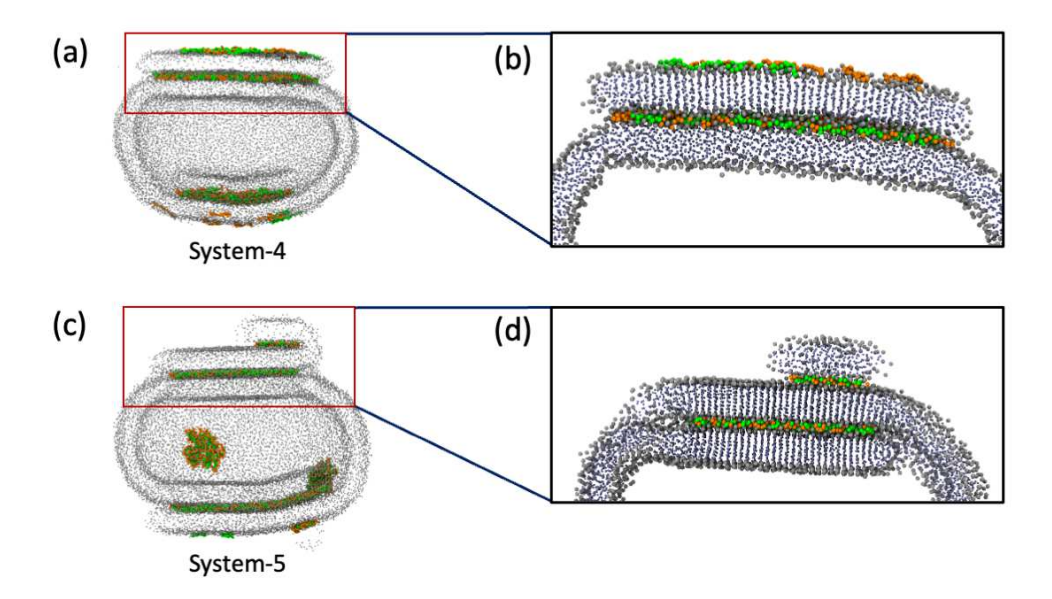


Figure 4: Emergence of multilamellar bilayer structures and local gelation by the act of phase separating polymer mixtures for system 4 (where $\varepsilon_{AB} = 1.0$, and $\varepsilon_{AH} = 2.0 = \varepsilon_{BH}$) and system 5 (where ε_{AB} , ε_{AH} , and ε_{BH} are the same and set to 2.0): (a) system 4, (b) cross-sectional and magnified view of 'a', (c) system 5, (d) cross-sectional and magnified view of 'c'. In the magnified views, the ordering of the lipid tails is highlighted in the vicinity of the polymers. The respective simulation movies are provided in **Supporting Information** [Video S5 and S6 for system-4 and system-5, respectively].

and grow. The detailed mechanism of endocytosis and exocytosis for both plant and animal cells is known and involve complex protein machineries for regulation.⁷⁰ However, such processes driven by simpler peptides or polymers have remained poorly characterized and understood. Similarly, multilamellar (or, multilayered/stacked) membranes might have various functional roles that are different from unilamellar membranes, as they provide a greater surface area.⁷¹ However, the origin behind the formation of such structures induced by LLPS is not well comprehended at present. In this paper, we have used solvent-free coarse-grained molecular dynamics simulation and unraveled the interplay among the key intermolecular interactions which can give rise to complex membrane and vesicle remodelings observed in recent experiments.^{17,18}

We have observed that a comparable interaction strength between the polymer-polymer and polymer-lipid pairs allows the formation of a coat around the membrane without significantly altering its morphology (Systems 1 and 2). On the other hand, for a successful event of endocytosis/exocytosis, a strong polymer-lipid interaction is not necessarily the key requirement; in fact, we find that the interpolymeric attractive interactions need to be much stronger than the polymer-lipid interactions (System 3). Such a combination of parameters helps the coacervate to preserve its spherical shape and at the same time drives the system toward an enthalpic minimum by adsorption followed by engulfment of the droplet. This is also associated with the critical size of the coacervate droplet, which in our model is found to be made of at least 46 polymers or more. We have connected our numerical results with existing continuum model-based theories. In addition to this, we have found the emergence of multilayered bilayer structures when the polymer-lipid interactions are considerably higher than the inter-polymeric attractions. For such systems, we have observed the multilayered bilayer associated with a local gel-like ordering in the vicinity of the polymer coats. The local gelation helps reduce the area per lipid and gain enthalpic stabilization. This can be used to modulate the spatial stiffness of a mono-component lipid vesicle and generate patchy functional properties (Systems 4 and 5).

Understanding the key intermolecular forces behind the LLPS-induced encapsulation, endocytosis, exocytosis, membrane bud formation, multilayered bilayer formation, and enhanced local ordering has broad implications. Our model study provides valuable guidance to the design of such coacervate-forming polymers for the desired extent of lipid vesicle remodeling. By focusing on simple models, our study provides a minimal parameter space with a high degree of tunability, which has potential impact on biomedicine, tissue engineering, and synthetic biology. One interesting application could be the design of coacervates as nano-carriers for drug delivery, ³⁸ in which medically important charged molecules/particles can be coated with such polymer mixtures to allow them to be engulfed by the cells. Another major interaction between coacervates and cell membranes is the formation of a layer around individual cells or clusters of cells, which can help protect the cells from harsh environmental conditions (such as pH shocks) or other external stresses, ⁶¹ a method routinely used in food

processing industries.⁶² Many applications, such as drug delivery, biosensing, and biomimetic systems can take advantage of patchy functional lipid vesicles. These patches can be functionalized with various molecules, such as proteins, peptides, antibodies, or nucleic acids, to create specific interactions with target molecules or cells, increasing the precision and potency of the substance. In biomimetic systems, they can be utilized to produce synthetic cell-like structures with particular functionalities, such as signaling or metabolic pathways.

Nonetheless, several questions remain to be addressed. In the future, we aim to explore the impact of bilayer composition and the parameter space that controls the sign of membrane curvature generated by the IDPs. Additionally, factors that control the LLPS-induced ordering of lipids certainly deserves further attention and will be analyzed thoroughly in future work.

Acknowledgement

We thank Dr. David Stelter for useful discussions while setting up the lipid model. This work was supported in part by grant NSF-CHE-2154804 to QC. Computational resources from the Extreme Science and Engineering Discovery Environment(XSEDE),⁷² which is supported by NSF Grant ACI-1548562, are greatly appreciated; part of the computational work was performed on the Shared Computing Cluster which is administered by Boston University's Research Computing Services (URL: www.bu.edu/tech/support/research/). SM thanks Boston University for providing the Adobe Photoshop license which is used to prepare Figures 3b, 3c, and the TOC.

Supporting Information Available

In the **Supporting Information** we provide the simulation movies for the processes shown in Figures 2 (Video S1, S2, S3, and S4) and 4 (Video S5 and S6).

Conflict of Interest Disclosure

The authors declare no competing financial interest.

References

- (1) Hyman, A. A.; Weber, C. A.; Jülicher, F. Liquid-liquid Phase Separation in Biology. *Annu. Rev. Cell Dev. Biol.* **2014**, *30*, 39–58.
- (2) Posey, A. E.; Holehouse, A. S.; Pappu, R. V. Phase Separation of Intrinsically Disordered Proteins. *Meth. Enzymol.* **2018**, *611*, 1–30.
- (3) McCarty, J.; Delaney, K. T.; Danielsen, S. P.; Fredrickson, G. H.; Shea, J.-E. Complete Phase Diagram for Liquid–liquid Phase Separation of Intrinsically Disordered Proteins. *J. Phys. Chem. Lett.* **2019**, *10*, 1644–1652.
- (4) Dinic, J.; Marciel, A. B.; Tirrell, M. V. Polyampholyte Physics: Liquid-liquid Phase Separation and Biological Condensates. *Curr. Opin. Colloid Interface Sci.* **2021**, *54*, 101457.
- (5) Alberti, S.; Dormann, D. Liquid-liquid Phase Separation in Disease. *Annu. Rev. Genet.* **2019**, *53*, 171–194.
- (6) Banani, S. F.; Lee, H. O.; Hyman, A. A.; Rosen, M. K. Biomolecular Condensates: Organizers of Cellular Biochemistry. *Nat. Rev. Mol. Cell. Biol.* **2017**, *18*, 285–298.
- (7) Molliex, A.; Temirov, J.; Lee, J.; Coughlin, M.; Kanagaraj, A. P.; Kim, H. J.; Mittag, T.; Taylor, J. P. Phase Separation by Low Complexity Domains Promotes Stress Granule Assembly and Drives Pathological Fibrillization. *Cell* **2015**, *163*, 123–133.
- (8) Banjade, S.; Rosen, M. K. Phase Transitions of Multivalent Proteins can Promote Clustering of Membrane Receptors. *eLife* **2014**, *3*, e04123.
- (9) Case, L. B.; Ditlev, J. A.; Rosen, M. K. Regulation of Transmembrane Signaling by Phase Separation. *Annu. Rev. Biophys.* **2019**, *48*, 465–494.
- (10) Kusumaatmaja, H.; May, A. I.; Knorr, R. L. Intracellular Wetting Mediates Contacts Between Liquid Compartments and Membrane-bound Organelles. *J. Cell Biol.* **2021**, 220, e202103175.
- (11) Huang, W. Y. C.; Alvarez, S.; Kondo, Y.; Lee, Y. K.; Chung, J. K.; Lam, H. Y. M.; Biswas, K. H.; Kuriyan, J.; Groves, J. T. A Molecular Assembly Phase Transition and Kinetic Proofreading Modulate Ras Activation by SOS. *Science* **2019**, *363*, 1098–1103.
- (12) Case, L. B.; Zhang, X.; Ditlev, J. A.; Rosen, M. K. Stoichiometry Controls Activity of Phase-separated Clusters of Actin Signaling Proteins. *Science* **2019**, *363*, 1093–1097.

- (13) Mondal, S.; Cui, Q. Coacervation of Poly-electrolytes in the Presence of Lipid Bilayers: Mutual Alteration of Structure and Morphology. *Chem. Sci.* **2022**, *13*, 7933–7946.
- (14) Yuan, F.; Alimohamadi, H.; Bakka, B.; Trementozzi, A. N.; Day, K. J.; Fawzi, N. L.; Rangamani, P.; Stachowiak, J. C. Membrane Bending by Protein Phase Separation. *Proc. Natl. Acad. Sci. U.S.A.* **2021**, *118*, e2017435118.
- (15) Day, K. J.; Kago, G.; Wang, L.; Richter, J. B.; Hayden, C. C.; Lafer, E. M.; Stachowiak, J. C. Liquid-like Protein Interactions Catalyse Assembly of Endocytic Vesicles. *Nat. Cell Biol.* **2021**, *23*, 366–376.
- (16) Bergeron-Sandoval, L.-P.; Kumar, S.; Heris, H. K.; Chang, C. L. A.; Cornell, C. E.; Keller, S. L.; Francois, P.; Hendricks, A. G.; Ehrlicher, A. J.; Pappu, R. V.; Michnick, S. W. Endocytic Proteins with Prion-like Domains form Viscoelastic Condensates that Enable Membrane Remodeling. *Proc. Natl. Acad. Sci. U.S.A.* 2021, 118, e2113789118.
- (17) Lu, T.; Liese, S.; Schoenmakers, L.; Weber, C. A.; Suzuki, H.; Huck, W. T.; Spruijt, E. Endocytosis of Coacervates into Liposomes. J. Am. Chem. Soc. 2022, 144, 13451–13455.
- (18) Allolio, C.; Magarkar, A.; Jurkiewicz, P.; Baxová, K.; Javanainen, M.; Mason, P. E.; Šachl, R.; Cebecauer, M.; Hof, M.; Horinek, D.; others Arginine-rich Cell-Penetrating Peptides Induce Membrane Multilamellarity and Subsequently Enter via Formation of a Fusion Pore. *Proc. Natl. Acad. Sci. U.S.A.* **2018**, *115*, 11923–11928.
- (19) Agudo-Canalejo, J.; Schultz, S. W.; Chino, H.; Migliano, S. M.; Saito, C.; Koyama-Honda, I.; Stenmark, H.; Brech, A.; May, A. I.; Mizushima, N.; Knorr, R. L. Wetting Regulates Autophagy of Phase-separated Compartments and the Cytosol. *Nature* **2021**, 591, 142–146.
- (20) Paul, S.; Audhya, A.; Cui, Q. Molecular Mechanism of GTP Binding and Dimerization-induced Enhancement of Sar1-mediated Membrane Remodeling. *Proc. Natl. Acad. Sci. U.S.A.* **2023**, *120*, e2212513120.
- (21) Kozlov, M. M.; Taraska, J. W. Generation of Nanoscopic Membrane Curvature for Membrane Trafficking. *Nat. Rev. Mol. Cell Biol.* **2022**, 1–16.
- (22) Lipowsky, R.; Döbereiner, H.-G.; Hiergeist, C.; Indrani, V. Membrane Curvature Induced by Polymers and Colloids. *Phys. A: Stat. Mech. Appl.* **1998**, *249*, 536–543.
- (23) Hicks, A.; Escobar, C. A.; Cross, T. A.; Zhou, H.-X. Fuzzy Association of an Intrinsically Disordered Protein with Acidic Membranes. *JACS Au* **2021**, *1*, 66–78.
- (24) Smrt, S. T.; Escobar, C. A.; Dey, S.; Cross, T. A.; Zhou, H.-X. An Arg/Ala-rich Helix in the N-terminal Region of M. Tuberculosis FtsQ is a Potential Membrane Anchor of the Z-ring. *Comm. Biol.* **2023**, *6*, 311.

- (25) Bremer, A.; Farag, M.; Borcherds, W. M.; Peran, I.; Martin, E. W.; Pappu, R. V.; Mittag, T. Deciphering how Naturally Occurring Sequence Features Impact the Phase Behaviours of Disordered Prion-like Domains. *Nat. Chem.* **2022**, *14*, 196–207.
- (26) Dignon, G. L.; Zheng, W.; Kim, Y. C.; Best, R. B.; Mittal, J. Sequence Determinants of Protein Phase Behavior From a Coarse-grained Model. *PLoS Comput. Biol.* **2018**, 14, e1005941.
- (27) Quiroz, F. G.; Chilkoti, A. Sequence Heuristics to Encode Phase Behaviour in Intrinsically Disordered Protein Polymers. *Nat. Mater.* **2015**, *14*, 1164–1171.
- (28) Schuster, B. S.; Dignon, G. L.; Tang, W. S.; Kelley, F. M.; Ranganath, A. K.; Jahnke, C. N.; Simpkins, A. G.; Regy, R. M.; Hammer, D. A.; Good, M. C.; others Identifying Sequence Perturbations to an Intrinsically Disordered Protein that Determine Its Phase-separation Behavior. *Proc. Natl. Acad. Sci. U.S.A.* **2020**, *117*, 11421–11431.
- (29) Chung, J. K.; Huang, W. Y. C.; Carbone, C. B.; Nocka, L. M.; Parikh, A. N.; Vale, R. D.; Groves, J. T. Coupled Membrane Lipid Miscibility and Phosphotyrosine-driven Protein Condensation Phase Transitions. *Biophys. J.* **2021**, *120*, 1257–1265.
- (30) Case, L. B.; M. De Pasquale; Henry, L.; Rosen, M. K. Synergistic Phase Separation of Two Pathways Promotes Integrin Clustering and Nascent Adhesion Formation. *eLife* **2022**, *11*, e72588.
- (31) Rouches, M.; Veatch, S. L.; Machta, B. B. Surface Densities Prewet a Near-critical Membrane. *Proc. Natl. Acad. Sci. U.S.A.* **2021**, *118*, e2103401118.
- (32) Liu, Z.; Yethiraj, A.; Cui, Q. Sensitive and Selective Polymer Condensation at Membrane Surface Driven by Positive Co-operativity. *Proc. Natl. Acad. Sci. U.S.A.* **2023**, 120, e2212516120.
- (33) Rumyantsev, A. M.; Jackson, N. E.; De Pablo, J. J. Polyelectrolyte Complex Coacervates: Recent Developments and New Frontiers. *Annu. Rev. Condens. Matter Phys.* **2021**, *12*, 155–176.
- (34) Sing, C. E.; Perry, S. L. Recent Progress in the Science of Complex Coacervation. *Soft Matter* **2020**, *16*, 2885–2914.
- (35) Delaney, K. T.; Fredrickson, G. H. Theory of Polyelectrolyte Complexation—Complex Coacervates are Self-coacervates. J. Chem. Phys. 2017, 146, 224902.
- (36) Melnyk, A.; Namieśnik, J.; Wolska, L. Theory and Recent Applications of Coacervate-based Extraction Techniques. *Trends Anal. Chem.* **2015**, *71*, 282–292.
- (37) Blocher, W. C.; Perry, S. L. Complex Coacervate-based Materials for Biomedicine. Wiley Interdiscip. Rev. Nanomed. Nanobiotechnol. 2017, 9, e1442.

- (38) Wang, Y.; Huang, L.; Shen, Y.; Tang, L.; Sun, R.; Shi, D.; Webster, T. J.; Tu, J.; Sun, C. Electrostatic Interactions between Polyglutamic Acid and Polylysine Yields Stable Polyion Complex Micelles for Deoxypodophyllotoxin Delivery. *Intl. J. Nanomed.* **2017**, *12*, 7963.
- (39) Hwang, J. J.; Stupp, S. I. Poly (amino acid) Bioadhesives for Tissue Repair. J. Biomater. Sci. Polym. Ed. 2000, 11, 1023–1038.
- (40) Richert, L.; Arntz, Y.; Schaaf, P.; Voegel, J.-C.; Picart, C. pH Dependent Growth of Poly (L-lysine)/ Poly (L-glutamic) Acid Multilayer Films and Their Cell Adhesion Properties. Surf. Sci. 2004, 570, 13–29.
- (41) Van Stevendaal, M. H.; Vasiukas, L.; Yewdall, N. A.; Mason, A. F.; van Hest, J. C. Engineering of Biocompatible Coacervate-based Synthetic Cells. ACS Appl. Mat. Interfaces 2021, 13, 7879–7889.
- (42) Wu, H.; Qiao, Y. Engineering Coacervate Droplets Towards the Building of Multiplex Biomimetic Protocells. *Supramolec. Mat.* **2022**, 100019.
- (43) Wang, B.; Zhang, L.; Bae, S. C.; Granick, S. Nanoparticle-induced Surface Reconstruction of Phospholipid Membranes. *Proc. Natl. Acad. Sci. U.S.A.* **2008**, *105*, 18171–18175.
- (44) Lee, Y.; Park, S.; Yuan, F.; Hayden, C. C.; Choi, S. Q.; Stachowiak, J. C. Lateral Compression of Lipids Drives Transbilayer Coupling of Liquid-like Protein Condensates. bioRxiv 2022, 2022–12.
- (45) Mangiarotti, A.; Chen, N.; Zhao, Z.; Lipowsky, R.; Dimova, R. Membrane Wetting, Molding and Reticulation by Protein Condensates. *bioRxiv* **2022**, 2022–06.
- (46) Nguemaha, V.; Zhou, H.-X. Liquid-liquid Phase Separation of Patchy Particles Illuminates Diverse Effects of Regulatory Components on Protein Droplet Formation. *Sci. Rep.* **2018**, *8*, 1–11.
- (47) Mazarakos, K.; Zhou, H.-X. Multiphase Organization is a Second Phase Transition Within Multi-component Biomolecular Condensates. *J. Chem. Phys.* **2022**, *156*, 191104.
- (48) Tsanai, M.; Frederix, P. W.; Schroer, C. F.; Souza, P. C.; Marrink, S. J. Coacervate Formation Studied by Explicit Solvent Coarse-grain Molecular Dynamics with the Martini Model. *Chem. Sci.* **2021**, *12*, 8521–8530.
- (49) Cooke, I. R.; Kremer, K.; Deserno, M. Tunable Generic Model for Fluid Bilayer Membranes. *Phys. Rev. E* **2005**, *72*, 011506.
- (50) Wu, Z.; Cui, Q.; Yethiraj, A. A New Coarse-grained Model for Water: the Importance of Electrostatic Interactions. *J. Phys. Chem. B* **2010**, *114*, 10524–10529.

- (51) Samanta, H. S.; Chakraborty, D.; Thirumalai, D. Charge Fluctuation Effects on the Shape of Flexible Polyampholytes with Applications to Intrinsically Disordered Proteins. J. Chem. Phys. 2018, 149, 163323.
- (52) Lin, Y.-H.; Song, J.; Forman-Kay, J. D.; Chan, H. S. Random-phase-approximation Theory for Sequence-dependent, Biologically Functional Liquid-liquid Phase Separation of Intrinsically Disordered Proteins. *J. Mol. Liq.* **2017**, *228*, 176–193.
- (53) Vácha, R.; Martinez-Veracoechea, F. J.; Frenkel, D. Receptor-mediated Endocytosis of Nanoparticles of Various Shapes. *Nano Lett.* **2011**, *11*, 5391–5395.
- (54) Spangler, E. J.; Upreti, S.; Laradji, M. Partial Wrapping and Spontaneous Endocytosis of Spherical Nanoparticles by Tensionless Lipid Membranes. *J. Chem. Phys.* **2016**, *144*, 044901.
- (55) Farag, M.; Cohen, S. R.; Borcherds, W. M.; Bremer, A.; Mittag, T.; Pappu, R. V. Condensates Formed by Prion-like Low-complexity Domains have Small-world Network Structures and Interfaces Defined by Expanded Conformations. *Nat. Comm.* **2022**, *13*, 7722.
- (56) Martínez, L.; Andrade, R.; Birgin, E. G.; Martínez, J. M. PACKMOL: A Package for Building Initial Configurations for Molecular Dynamics Simulations. *J. Comput. Chem.* **2009**, *30*, 2157–2164.
- (57) Thompson, A. P.; Aktulga, H. M.; Berger, R.; Bolintineanu, D. S.; Brown, W. M.; Crozier, P. S.; in't Veld, P. J.; Kohlmeyer, A.; Moore, S. G.; Nguyen, T. D.; others LAMMPS-a Flexible Simulation Tool for Particle-based Materials Modeling at the Atomic, Meso, and Continuum Scales. *Comput. Phys. Comm.* **2022**, *271*, 108171.
- (58) Plimpton, S. Fast parallel algorithms for short-range molecular dynamics. *J. Comp. Phys.* **1995**, *117*, 1–19.
- (59) Humphrey, W.; Dalke, A.; Schulten, K. VMD: Visual Molecular Dynamics. J. Mol. Graph. 1996, 14, 33–38.
- (60) Huang, J.; Rauscher, S.; Nawrocki, G.; Ran, T.; Feig, M.; De Groot, B. L.; Grubmüller, H.; MacKerell, A. D. CHARMM36m: An Improved Force Field for Folded and Intrinsically Disordered Proteins. *Nat. Meth.* **2017**, *14*, 71–73.
- (61) Quemeneur, F.; Rinaudo, M.; Maret, G.; Pépin-Donat, B. Decoration of Lipid Vesicles by Polyelectrolytes: Mechanism and Structure. *Soft Matter* **2010**, *6*, 4471–4481.
- (62) Devi, N.; Sarmah, M.; Khatun, B.; Maji, T. K. Encapsulation of Active Ingredients in Polysaccharide–Protein Complex Coacervates. *Adv. Colloid Interface Sci.* **2017**, *239*, 136–145.
- (63) Deserno, M. Elastic Deformation of a Fluid Membrane upon Colloid Binding. *Phys. Rev. E* **2004**, *69*, 031903.

- (64) Bahrami, A. H.; Lipowsky, R.; Weikl, T. R. The Role of Membrane Curvature for the Wrapping of Nanoparticles. *Soft Matter* **2016**, *12*, 581–587.
- (65) Jho, Y.; Yoo, H. Y.; Lin, Y.; Han, S.; Hwang, D. S. Molecular and Structural Basis of Low Interfacial Energy of Complex Coacervates in Water. *Adv. Colloid Interface Sci.* **2017**, *239*, 61–73.
- (66) Taylor, N.; Elbaum-Garfinkle, S.; Vaidya, N.; Zhang, H.; Stone, H. A.; Brangwynne, C. P. Biophysical Characterization of Organelle-based RNA/Protein Liquid Phases Using Microfluidics. *Soft Matt.* **2016**, *12*, 9142–9150.
- (67) Lipowsky, R. Spontaneous Tubulation of Membranes and Vesicles Reveals Membrane Tension Generated by Spontaneous Curvature. *Faraday Diss.* **2013**, *161*, 305–331.
- (68) Lipowsky, R. Multispherical Shapes of Vesicles Highlight the Curvature Elasticity of Biomembranes. *Adv. Colloid Interface Sci.* **2022**, *301*, 102613.
- (69) Piskulich, Z. A.; Cui, Q. Machine Learning-Assisted Phase Transition Temperatures from Generalized Replica Exchange Simulations of Dry Martini Lipid Bilayers. *J. Phys. Chem. Lett.* **2022**, *13*, 6481–6486.
- (70) Wu, L.-G.; Hamid, E.; Shin, W.; Chiang, H.-C. Exocytosis and Endocytosis: Modes, Functions, and Coupling Mechanisms. *Annu. Rev. Physiol.* **2014**, *76*, 301.
- (71) Heath, G. R.; Li, M.; Rong, H.; Radu, V.; Frielingsdorf, S.; Lenz, O.; Butt, J. N.; Jeuken, L. J. Multilayered Lipid Membrane Stacks for Biocatalysis Using Membrane Enzymes. *Adv. Funct. Mat.* **2017**, *27*, 1606265.
- (72) Towns, J.; Cockerill, T.; Dahan, M.; Foster, I.; Gaither, K.; Grimshaw, A.; Hazelwood, V.; Lathrop, S.; Lifka, D.; Peterson, G. D.; Roskies, R.; Scott, J. R.; Wilkins-Diehr, N. XSEDE: Accelerating Scientific Discovery. *Comput Sci. & Engn.* **2014**, *16*, 62–74.